Engineering 30 (2023) 49–54

Contents lists available at ScienceDirect

Engineering

journal homepage: www.elsevier.com/locate/eng

Research
Microwave Wireless Power Transfer Technology—Article

Synthesized All-Pass Waveguide for Ultrafast Electronics

Desong Wang, Ke Wu *

Poly-Grames Research Center, Department of Electrical Engineering, Polytechnique Montréal, Montreal, QC H3T 1J4, Canada

ARTICLE INFO

Article history:
Received 4 August 2022
Revised 31 January 2023
Accepted 9 April 2023
Available online 6 May 2023

Keywords:
All-pass waveguide
Ultrashort pulse
Picosecond transmission
Ultrafast electronics
Terahertz technology
Mode-selective transmission line

ABSTRACT

Ultrashort pulse transmission has been recognized as a primary problem that fundamentally hinders the development of ultrafast electronics beyond the current nanosecond timescale. This requires a transmission line or waveguide that exhibits an all-pass frequency behavior for the transmitted ultrashort pulse signals. However, this type of waveguiding structure has not yet been practically developed; groundbreaking innovations and advances in signal transmission technology are urgently required to address this scenario. Herein, we present a synthesized all-pass waveguide that demonstrates record guided-wave controlling capabilities, including eigenmode reshaping, polarization rotation, loss reduction, and dispersion improvement. We experimentally developed two waveguides for use in ultrabroad frequency ranges (direct current (DC)-to-millimeter-wave and DC-to-terahertz). Our results suggest that the waveguides can efficiently transmit picosecond electrical pulses while maintaining signal integrity. This waveguide technology is an important breakthrough in the evolution of ultrafast electronics, providing a path towards frequency-engineered ultrashort pulses for low-loss and low-dispersion transmissions.

1. Introduction

Ultrafast electronics is prominent in emerging ultrafast phenomena-focused sciences and technologies, particularly on the picosecond and sub-picosecond timescales [1,2]. It has a wide range of applications in many fields, such as basic science [3], terahertz (THz) detection [4], imaging [5], high-frequency measurement [6], high-capability communication [7], and biology and medicine [8]. This has attracted interest to the most critical problem: ultrashort electrical pulse transmission [9–11]. In particular, a transmission line or waveguide is required to support low-loss, low-dispersion, and all-pass guidance for ultrabroadband signals (direct current (DC)-to-millimeter-wave (mmW) or DC-to-THz) [12,13]. However, all well-known transmission media suffer from the negative effects of dispersion and loss in connection with a low-frequency cutoff (high-pass) [14] and/or high-frequency attenuation (low-pass) [15].

Commonly used planar transmission lines, such as microstrip lines [16], coplanar waveguides (CPWs) [17], and striplines [18], which operate in a ground-plane-referenced transverse electromagnetic (TEM) or quasi-TEM mode, exhibit an inherent low-pass ability to transmit broadband signals beginning from DC (or a very low frequency). Nevertheless, they suffer from weak field confinement and near-monotonically increasing attenuation with frequency. This is in contrast to the most popular integrated waveguides currently in use, including dielectric waveguides [19,20] and substrate-integrated waveguides (SIWs) [21,22], which operate in a dominant transverse electric (TE), transverse magnetic (TM), or even hybrid mode. They have a relatively low attenuation but have a low-frequency cutoff, thus yielding a strong dispersion over a certain frequency range. These fundamental properties are primarily a result of the guided-wave nature of the respective dominant eigenmodes (eigenfields), which are generally assumed to remain unchanged for a given waveguide cross-section. In other words, none of these conventional transmission media can create an all-pass distortion-free signal transmission that covers the DC-to-THz ultrabroad bandwidth in the frequency domain. Revolutionary innovations and advances in signal transmission technology are required to address this problem [23–25]. This is the most fundamental challenge in the future development of ultrafast electronics in support of picosecond or shorter pulse generation [26], transmission [27], and processing [28], which requires breaking through the current nanosecond electronics barrier.

The information-carrying capacity of a transmission system is limited by the dispersion and attenuation characteristics of the dominant propagating mode over the bandwidth of interest. Given the aforementioned nonidealities of the specific eigenmodes, it is

* Corresponding author.
E-mail address: ke.wu@polymtl.ca (K. Wu).

https://doi.org/10.1016/j.eng.2023.04.005

intuitive to propose that if we could reshape a propagating mode as desired, we would be able to deliberately control the propagation of guided waves. For a given guide, the modal eigenvalues are unique solutions to Maxwell's equations corresponding to specific boundary conditions [29]. Nonetheless, note that these solutions are a function of frequency, which enables us to "construct" particular eigenmodes with frequency [30] and thus obtain various desired modal behaviors. In our previous study, we attempted to change the dominant mode of a uniform transmission line [13,31]. However, the mode change is not well reflected in the related frequency characteristics (specifically, high-frequency attenuation, frequency dispersion, and wave polarization).

In this article, we demonstrate a synthesized waveguide (S-WG) technology that supports ultrashort electrical pulse transmission on an unprecedented picosecond scale. This waveguide has a dominant mode that is fully reshaped with frequency. Therefore, we can manipulate its guided wave properties, including the polarization rotation, loss reduction, and dispersion improvement. These findings are revealed using two waveguide examples that were separately achieved in the mmW [32,33] and THz frequency ranges [34,35]. The numerical and experimental results of these S-WGs demonstrate their capabilities in efficiently guiding picosecond electrical pulses while effectively maintaining signal integrity.

2. Synthesized waveguide

The S-WG was constructed by symmetrically etching two narrow slits over the top plane of a rectangular waveguide filled with a dielectric of permittivity ε_1 and then covering them with another dielectric (or air) of permittivity ε_2. This simple geometric setting, as shown in Fig. 1(a), has important characteristics: transverse inhomogeneity ($\varepsilon_2 < \varepsilon_1$) and longitudinal invariance. It is compatible with planar fabrication processes and convenient for integration with other devices. Because of the engineered boundaries, this particular waveguide supports a frequency-varying dominant eigenmode that undergoes a gradual-to-complete conversion from a quasi-TEM CPW mode to a quasi-TE_{10} waveguide mode as the operating frequency increases (see Appendix A for eigenmode analysis). Hence, this S-WG merges the desired waveguiding properties offered by both the CPW (no cutoff frequency and horizontal polarization) and rectangular waveguide (low transmission loss and vertical polarization). This special scenario is briefly described in the block diagram shown in Fig. 1(b). Regarding the specific frequency point labeled f_c in this figure, interested readers can refer to the detailed discussions in Refs. [36,37].

To illustrate the frequency-dependent mode conversion, we examined the electric fields over the cross-section of the waveguide at different frequencies (Fig. 1(c)). As the frequency continues to increase, the electric fields evolve from being concentrated around the top slits to being distributed over the entire cross-section, and the polarization (direction of the main electric fields) rotates by 90° (from horizontal to vertical). In other words, both the field pattern and polarization direction are subject to vivid changes with frequency, which is significantly different from their relatively stationary counterparts in conventional waveguiding structures (Fig. S1 in Appendix A). The special modal characteristics of the S-WG offer many unique advantages over common waveguide structures, such as ultrabroad operating bandwidth, reduced high-frequency loss, and low signal dispersion. Figs. 1(d) and (e) compare the propagation constants of the S-WG and its counterparts. As expected, both the SIW and dielectric waveguide exhibit a low-frequency cutoff phenomenon (Fig. 1(d)); the CPW, stripline, and microstrip line suffer from relatively high losses,

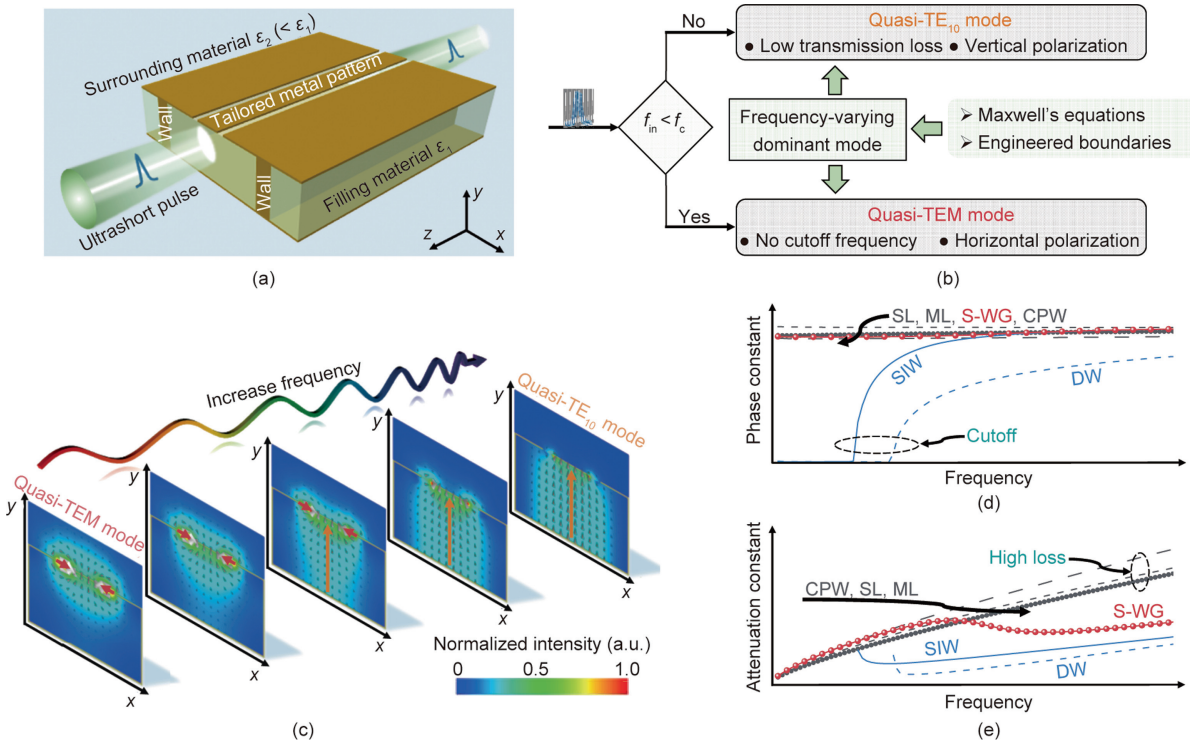

Fig. 1. Concept of synthesized all-pass waveguide. (a) Schematic of S-WG. (b) Frequency-dependent mode-conversion mechanism. The frequency-varying dominant mode behaves as a quasi-TEM or quasi-TE_{10} mode depending on whether the frequency of a guided wave f_{in} is lower or higher than a specific frequency f_c, as a solution to Maxwell's equations together with engineered boundaries. Regarding f_c, detailed discussions are available in Refs. [36,37]. (c) Evolution of cross-sectional electric fields with frequency. The red and orange arrows represent the direction of main electric fields at different frequencies. (d, e) Comparison of phase and attenuation constants of S-WG and common transmission media including SIW, dielectric waveguide (DW), CPW, stripline (SL), and microstrip line (ML).

particularly at high frequencies (Fig. 1(e)). Additionally, we compared the S-WG with the mode-selective transmission line (MSTL) presented in our previous works [30,31,36,37] in terms of their field distributions and propagation constants (Fig. S2 in Appendix A). The comparison results show that the MSTL exhibits similar frequency-dependent modal behavior, but with a fixed polarization direction. Furthermore, its frequency characteristics, particularly the high-frequency attenuation and frequency dispersion, do not demonstrate a clear benefit from mode conversion. Fortunately, our S-WG overcomes these disadvantages, making it a promising candidate for transmitting ultrabroadband ultrashort pulses. The comparison results are summarized in Table S1 in Appendix A. To demonstrate the proof-of-principle, we developed two such S-WGs for use in ultrabroad frequency ranges, from DC to THz (300 GHz) and mmW (67 GHz).

3. Realization in the THz spectrum

We first implemented a microscale-S-WG on an alumina substrate for THz-wave guidance (Figs. 2(a)–(c)). To characterize the ultrabroad frequency response, we performed experiments separately over different frequency ranges using a THz probe station (Fig. 2(d)). The detailed fabrication and measurement procedures are presented in Appendix A. Fig. 2(e) shows the measured transmission and reflection responses of the fabricated circuit from 10 MHz (near DC) to 325 GHz. The transmission response was linear at frequencies up to 300 GHz, and the reflection curve remained below −10 dB. Fig. 2(f) shows the propagation constants of the S-WG, which were extracted from the measured scattering parameters. The normalized phase constant experienced an 18.5% change throughout the entire operating range, which was attributed to the variable modal behavior. The attenuation constant increased monotonically with frequency and reached a maximum value of 0.72 dB·mm^{-1}; however, at frequencies above approximately 170 GHz, a noticeable slowing down was observed. This phenomenon became more pronounced at larger distances between the bilateral sidewalls (Fig. S3 in Appendix A). The derived time-domain results (Fig. 2(g)) demonstrated that this waveguide supports the efficient transmission of an ultrashort pulse with a 2 ps full width at half maximum (FWHM) pulse duration. The numerical simulation results are plotted in Figs. 2(e)–(g) and were observed to be in close agreement with the experimental data.

To facilitate the experimental characterization, we designed a continuously tapered transition (Fig. 3(a)) to directly connect the S-WG to a grounded CPW (GCPW) with a fixed characteristic impedance of 50 Ω (Fig. 3(b)). This taper provided good impedance and field matching between the S-WG and GCPW [38,39], ensuring smooth power delivery (Fig. 3(c)). As shown in Fig. 3(d), an ultrashort pulse was launched on the GCPW side into the CPW mode, where the electric fields were primarily concentrated around the narrow slits. As the pulse propagated down the taper, power was smoothly delivered to the frequency-varying dominant mode of the S-WG on the other side. These results suggested that the variable dominant mode of the S-WG was excited with the aid of the taper.

4. Realization in the mmW spectrum

We evaluated the waveguiding capabilities in the mmW frequency range (DC to 67 GHz) to further verify the validity and generality of the S-WG concept. An mmW waveguide was implemented on a low-loss dielectric substrate and then loaded

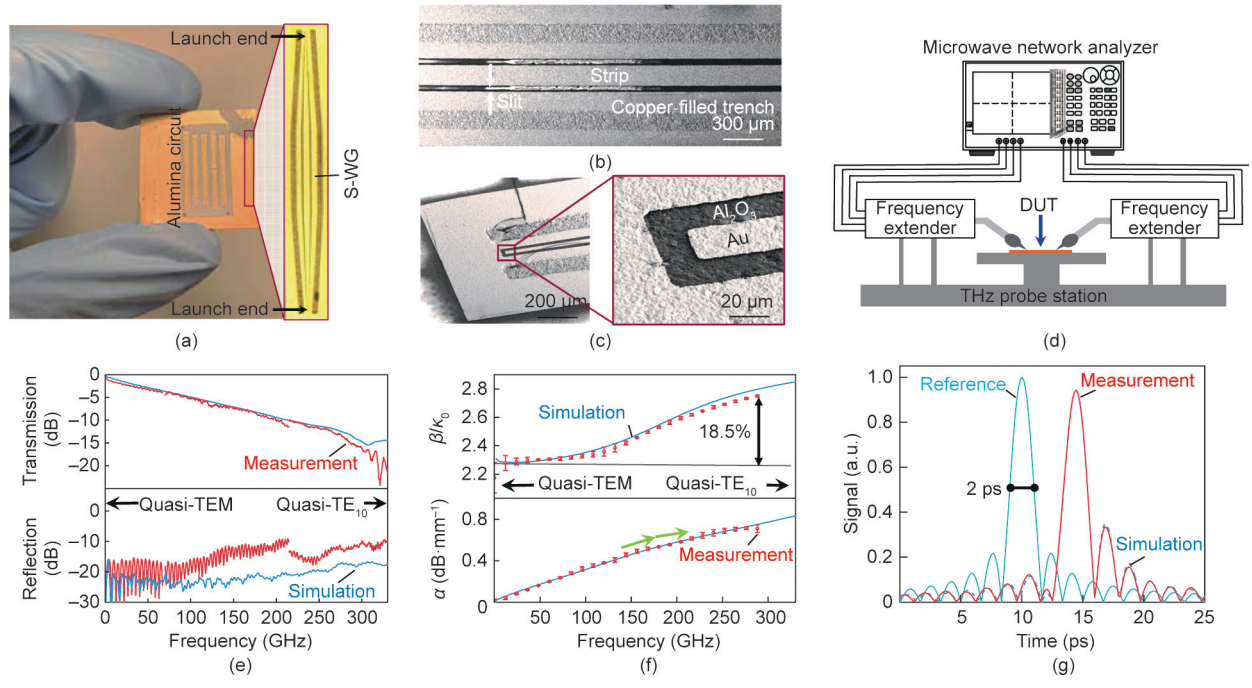

Fig. 2. Implementation of THz S-WG. (a) Micrographs of the fabricated samples on an alumina substrate. A single sample is magnified for a clear demonstration. Several back-to-back circuits of different lengths (including through-reflect-line (TRL) calibration kits) were fabricated together for experimental characterization. (b) Scanning electron microscope (SEM) image of the THz S-WG. (c) SEM images of the grounded CPW (GCPW) launch end. (d) Schematic of the experimental setup for frequency-domain characterization of the THz device under test (DUT). Note that for the measurement at frequencies below 67 GHz, the microwave network analyzer was connected directly to radiofrequency probes using 1.85 mm coaxial cables without the use of frequency extenders (Appendix A). (e) Measured and simulated (using finite-element modelling) transmission and reflection responses. These results are for a 14.4 mm-long back-to-back circuit (including effects of tapered transitions and GCPW launch ends). Several small discontinuities appear on the measurement curves at specific frequency points, which are a result of the waveguide characterization approach adopted (see Appendix A for more details). (f) Experimentally extracted and numerically simulated attenuation α and normalized phase constants β/k_0. β: phase constant; k_0: free-space propagation constant. The error bars indicate the experimental extraction uncertainty (±1 s.d. of three independent extractions, where s.d. represents the standard deviation from measurements). (g) Evolution of an ultrashort pulse with a 2 ps FWHM pulse duration as it propagates along the S-WG for 0.5 mm.

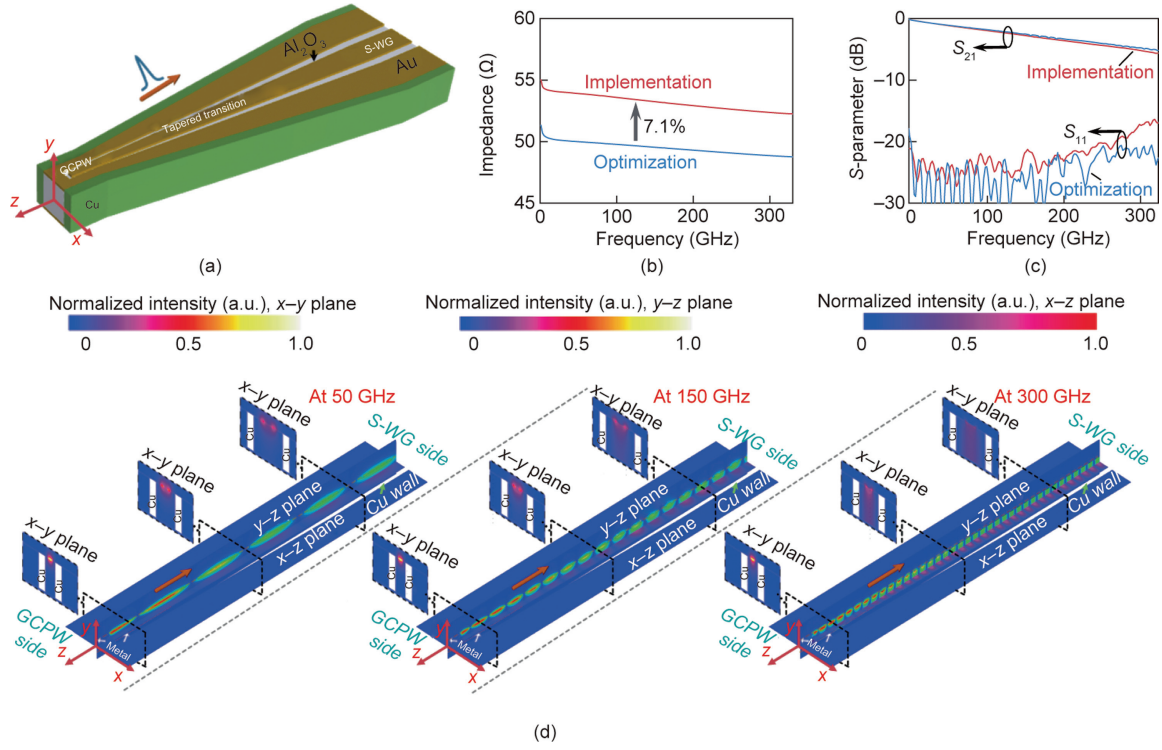

Fig. 3. Tapered transition design. (a) Schematic of tapered transition design. The taper connects the S-WG to a GCPW. (b) Characteristic impedance of the GCPW launch end. The finally implemented GCPW has a 7.1% increase in characteristic impedance compared with the originally optimized value. (c) Simulated transmission (S_{21}) and reflection (S_{11}) responses of the tapered transition. At frequencies up to 300 GHz, the S_{21} curve (in decibel scale) is linear, and the S_{11} curve remains below −18 dB, indicating smooth power delivery and good matching between the S-WG and GCPW. (d) Electric field distributions in the *x*–*z*, *y*–*z*, and *x*–*y* planes of the transition at 50, 150, and 300 GHz. The transition model is hidden to clearly show the field distributions in which the positions of metal layers and copper walls are marked for reference. The orange arrows indicate the propagation direction of guided waves. The fields on the GCPW side (CPW mode) are almost the same at different frequencies, whereas those on the S-WG side (frequency-varying mode) undergo a significant shape change.

with an electrically thin sheet on top (Fig. 4(a)). The primary aim of adding the superstrate was to increase the effective permittivity ε_2 of the surrounding material. The resulting ε_2 increased to approach but still less than that of the filling material ε_1 (i.e., $\varepsilon_2 < \varepsilon_1$). This meant that the frequency dispersion of this waveguide improved (Fig. 4(b)), while the geometric characteristics of the transverse inhomogeneity were preserved. In this case, bilateral sidewalls were implemented with periodically plated trenches that acted as continuous electric walls (Fig. S4 in Appendix A).

Similar to the THz S-WG, this mmW demonstration has a frequency-varying dominant mode (Figs. S5 and S6 in Appendix A) and thus exhibits superior performance. It does not lose generality and can easily be fabricated using a low-cost printed circuit board (PCB) process (Fig. S7 in Appendix A). We experimentally confirmed broadband signal transmission (10 MHz to 67 GHz, see Appendix A) using tapered transitions (Fig. 4(c)) constructed in the same manner as in the THz case. Fig. 4(d) compares the numerically simulated and experimentally measured frequency responses of the fabricated back-to-back circuit (Fig. 4(c)). The transmission responses indicated that the insertion loss increased gradually with frequency; however, this increase slowed down in the right half of the frequency plane. The reflection level was maintained below −10 dB, indicating good matching over the operating bandwidth. Fig. 4(e) shows the extracted propagation constants of the S-WG. This mmW waveguide had a smaller change (< 5.6%) in its normalized phase constant compared with the THz waveguide (Fig. 2(f)), implying an improvement in signal dispersion. The attenuation constant first increased with frequency; however, surprisingly, it decreased steadily after reaching a maximum value of 0.026 dB·mm^{-1} near 38 GHz, which ensured a low dissipative loss throughout. This was attributed to the frequency-dependent mode conversion that occurred in the S-WG. This distinctive attenuation phenomenon was reflected in the thermal effects (Fig. S8 in Appendix A). Fig. 4(f) plots the derived pulse responses, showing that a 9 ps FWHM pulse can be transmitted well through the mmW S-WG without distortion.

5. Conclusions

We developed a S-WG that enables the efficient guidance and proper manipulation of ultrashort electrical pulses. Through elaborate geometric tailoring, we conceived a waveguide whose dominant eigenmode was fully reshaped with frequency. Consequently, the guided wave underwent a polarization rotation of 90° and an anomalous but significant reduction in high-frequency loss while attaining superior dispersion property. To validate and demonstrate the potential and generality of this technology, we present two simple waveguide prototypes operating in different frequency ranges (DC to 67 and 300 GHz). Our results show that both waveguides can efficiently transmit picosecond pulses. Notably, the S-WG is highly scalable, possibly extending its applicability to frequencies above 1 THz and beyond (i.e., picosecond or sub-picosecond pulse bandwidth).

This study offers new avenues for the future development of ultrafast electronics, particularly in connection with ultrashort pulse transmission. The proposed waveguide technology is expected to become the backbone of future ultrafast electronic circuits, interconnects, and systems [40–42]. Despite the conspicuous superiority of the presented waveguiding technology, its practical applications still require more effort to further improve the excitation of the variable-dominant mode and the suppression of undesired modes.

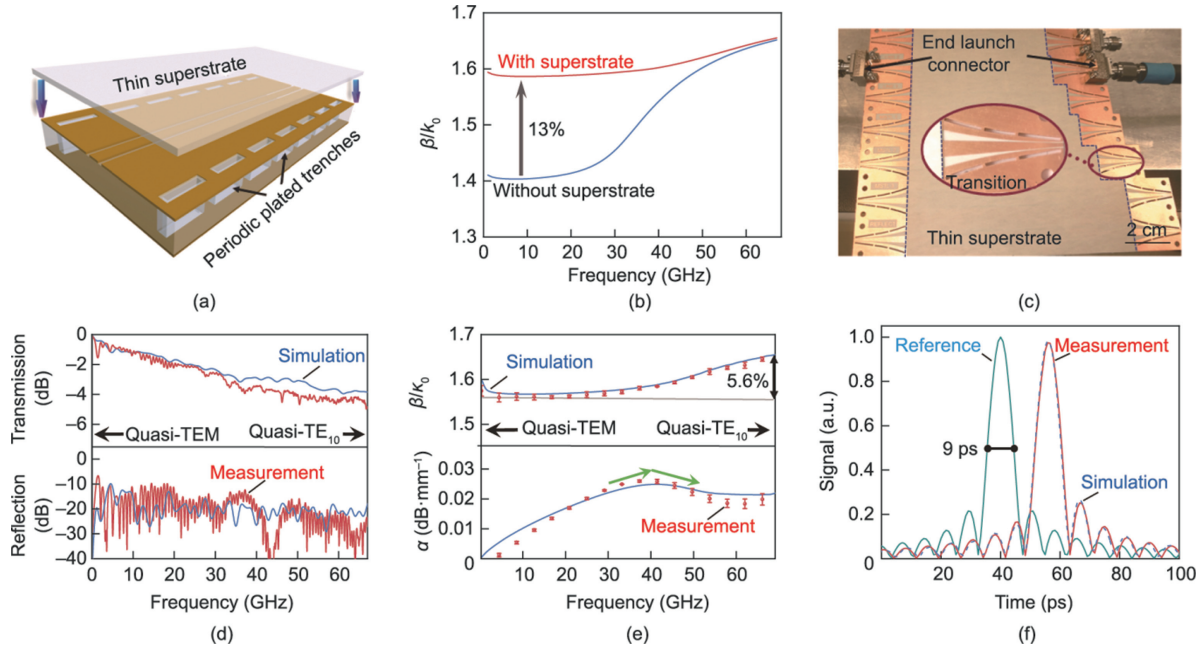

Fig. 4. Implementation of mmW S-WG. (a) Schematic of mmW S-WG. (b) Dispersion curve of the S-WG with and without a thin superstrate. The thin superstrate contributes significantly to increasing the normalized phase constant β/k_0 (or effective permittivity) in the low-frequency range (quasi-TEM mode) but has no noticeable effect on it at higher frequencies (quasi-TE_{10} mode). The flatter curve for the superstrate case indicates an improvement in signal dispersion. (c) Micrograph of the fabricated samples. A tapered transition is magnified for better demonstration. Several back-to-back circuits of different lengths (including TRL calibration kits) were fabricated together for experimental characterization. (d) Measured and simulated (via finite-element modelling) transmission and reflection responses. These results are for a 124 mm-long back-to-back circuit (including effects of tapered transitions and end launch connectors). (e) Experimentally extracted and numerically simulated attenuation α and normalized phase constants β/k_0. The error bars indicate the experimental extraction uncertainty (±1 s.d. of three independent extractions). (f) Evolution of an ultrashort pulse with a 9 ps FWHM pulse duration as it propagates along the S-WG for 3 mm.

Acknowledgments

We thank David Dousset for helping with the measurements at the terahertz probe station and Louis-Philippe Carignan for capturing the scanning electron microscope images. We are grateful to the technical staff of the Poly-Grames Research Center at Polytechnique Montreal for the circuit fabrication. We thank Sarah Wu Martinez for language editing. Desong Wang acknowledges discussions with Ben You, Muhibur Rahman, and Louis-Philippe Carignan. This study was supported in part by the Natural Sciences and Engineering Research Council of Canada (NSERC) Discovery Grant and in part by the NSERC–Huawei Industrial Research Chair Program.

Compliance with ethics guidelines

Desong Wang and Ke Wu declare that they have no conflict of interest or financial conflicts to disclose.

Appendix A. Supplementary data

Supplementary data to this article can be found online at https://doi.org/10.1016/j.eng.2023.04.005.

References

[1] Li N, Zhang B, He Y, Luo Y. Sub-picosecond nanodiodes for low-power ultrafast electronics. Adv Mater 2021;33(33):2100874.
[2] Nikoo MS, Jafari A, Perera N, Zhu M, Santoruvo G, Matioli E. Nanoplasma-enabled picosecond switches for ultrafast electronics. Nature 2020;579(7800):534–9.
[3] Yang Y, Wilson RB, Gorchon J, Lambert CH, Salahuddin S, Bokor J. Ultrafast magnetization reversal by picosecond electrical pulses. Sci Adv 2017;3(11):e1603117.
[4] Ferguson B, Zhang XC. Materials for terahertz science and technology. Nat Mater 2002;1:26–33.
[5] Cocker TL, Peller D, Yu P, Repp J, Huber R. Tracking the ultrafast motion of a single molecule by femtosecond orbital imaging. Nature 2016;539(7628):263–7.
[6] Kahrs M. 50 years of RF and microwave sampling. IEEE Trans Microw Theory Tech 2003;51(6):1787–805.
[7] Koenig S, Lopez-Diaz D, Antes J, Boes F, Henneberger R, Leuther A, et al. Wireless sub-THz communication system with high data rate. Nat Photon 2013;7(12):977–81.
[8] Siegel PH. Terahertz technology in biology and medicine. IEEE Trans Microw Theory Tech 2004;52(10):2438–47.
[9] Jhuria K, Hohlfeld J, Pattabi A, Martin E, Córdova AYA, Shi X, et al. Spin-orbit torque switching of a ferromagnet with picosecond electrical pulses. Nat Electron 2020;3(11):680–6.
[10] Spencer TJ, Osborn T, Kohl PA. High-frequency chip connections. Science 2008;320(5877):756–7.
[11] Hsiang TY, Whitaker JF, Sobolewski R, Dykaar DR, Mourou GA. Propagation characteristics of picosecond electrical transients on coplanar striplines. Appl Phys Lett 1987;51(19):1551–3.
[12] Yu X, Sugeta M, Yamagami Y, Fujita M, Nagatsuma T. Simultaneous low-loss and low-dispersion in a photonic-crystal waveguide for terahertz communications. Appl Phys Express 2019;12(1):012005.
[13] Fesharaki F, Djerafi T, Chaker M, Wu K. Low-loss and low-dispersion transmission line over DC-to-THz spectrum. IEEE Trans Terahertz Sci Technol 2016;6(4):611–8.
[14] McGowan RW, Gallot G, Grischkowsky D. Propagation of ultrawideband short pulses of terahertz radiation through submillimeter-diameter circular waveguides. Opt Lett 1999;24(20):1431–3.
[15] Zhang J, Alexandrou S, Hsiang TY. Attenuation characteristics of coplanar waveguides at subterahertz frequencies. IEEE Trans Microw Theory Tech 2005;53(11):3281–7.
[16] Roskos H, Nuss MC, Goossen KW, Kisker DW. Propagation of picosecond electrical pulses on a silicon-based microstrip line with buried cobalt silicide ground plane. Appl Phys Lett 1991;58(23):2604–6.
[17] Hattermann H, Bothner D, Ley LY, Ferdinand B, Wiedmaier D, Sárkány L, et al. Coupling ultracold atoms to a superconducting coplanar waveguide resonator. Nat Commun 2017;8:2254.

[18] Burchett MH, Pennock SR, Shepherd PR. A rigorous analysis of uniform stripline of arbitrary dimensions. IEEE Trans Microw Theory Tech 1993;41(12):2074–80.
[19] Yeh C, Shimabukuro F, Stanton P, Jamnejad V, Imbriale W, Manshadi F. Communication at millimetre–submillimetre wavelengths using a ceramic ribbon. Nature 2000;404(6778):584–8.
[20] Chaisakul P, Marris-Morini D, Frigerio J, Chrastina D, Rouifed MS, Cecchi S, et al. Integrated germanium optical interconnects on silicon substrates. Nat Photon 2014;8(6):482–8.
[21] Wu K, Cheng YJ, Djerafi T, Hong W. Substrate-integrated millimeter-wave and terahertz antenna technology. Proc IEEE 2012;100(7):2219–32.
[22] Zhou Z, Li Y, Li H, Sun W, Liberal I, Engheta N. Substrate-integrated photonic doping for near-zero-index devices. Nat Commun 2019;10:4132.
[23] Wang K, Mittleman D. Metal wires for terahertz wave guiding. Nature 2004;432(7015):376–9.
[24] Zhang Z, Chen Y, Cui S, He F, Chen M, Zhang Z, et al. Manipulation of polarizations for broadband terahertz waves emitted from laser plasma filaments. Nat Photon 2018;12(9):554–9.
[25] Lemoult F, Kaina N, Fink M, Lerosey G. Wave propagation control at the deep subwavelength scale in metamaterials. Nat Phys 2013;9:55–60.
[26] Chemla DS, Miller DAB, Schmitt-Rink S. Generation of ultrashort electrical pulses through screening by virtual populations in biased quantum wells. Phys Rev Lett 1987;59(9):1018–21.
[27] Frankel MY, Gupta S, Valdmanis JA, Mourou GA. Terahertz attenuation and dispersion characteristics of coplanar transmission lines. IEEE Trans Microw Theory Tech 1991;39(6):910–6.
[28] Hu Q, Joshi RP. Transmembrane voltage analyses in spheroidal cells in response to an intense ultrashort electrical pulse. Phys Rev E 2009;79:011901.
[29] Liberal I, Mahmoud AM, Engheta N. Geometry-invariant resonant cavities. Nat Commun 2016;7:10989.
[30] Wang D, Fesharaki F, Wu K. Physical evidence of mode conversion along mode-selective transmission line. In: Proceedings of 2017 IEEE MTT-S International Microwave Symposium (IMS); 2017 Jun 4–9; Honolulu, HI, USA; 2017.
[31] Wang D, Wu K. Propagation characteristics of mode-selective transmission line. In: Proceedings of 2018 IEEE MTT-S International Microwave Symposium (IMS); 2018 Jun 10–15; Philadelphia, PA, USA; 2018.
[32] Mittra R, Nasri A, Arya RK. Wide-angle scanning antennas for millimeter-wave 5G applications. Engineering 2022;11:60–71.
[33] Venkatesh S, Lu X, Tang B, Sengupta K. Secure space–time-modulated millimetre-wave wireless links that are resilient to distributed eavesdropper attacks. Nat Electron 2021;4(11):827–36.
[34] Tonouchi M. Cutting-edge terahertz technology. Nat Photon 2007;1(2):97–105.
[35] Huang Y, Shen Y, Wang J. From terahertz imaging to terahertz wireless communications. Engineering 2023;22:106–24.
[36] Wang D, Fesharaki F, Wu K. Longitudinally uniform transmission lines with frequency-enabled mode conversion. IEEE Access 2018;6:24089–109.
[37] Wang D, Wu K. Mode-selective transmission line—Part I: theoretical foundation and physical mechanism. IEEE Trans Compon Packag Manuf Technol 2020;10(12):2072–86.
[38] Johnson SG, Bienstman P, Skorobogatiy MA, Ibanescu M, Lidorikis E, Joannopoulos JD. Adiabatic theorem and continuous coupled-mode theory for efficient taper transitions in photonic crystals. Phys Rev E 2002;66(6): 066608.
[39] Wang D, Wu K. Mode-selective transmission line—Part II: excitation scheme and experimental verification. IEEE Trans Compon Packag Manuf Technol 2021;11(2):260–72.
[40] Sengupta K, Nagatsuma T, Mittleman DM. Terahertz integrated electronic and hybrid electronic–photonic systems. Nat Electron 2018;1(12):622–35.
[41] Tataria H, Shafi M, Molisch AF, Dohler M, Sjöland H, Tufvesson F. 6G wireless systems: vision, requirements, challenges, insights, and opportunities. Proc IEEE 2021;109(7):1166–99.
[42] Lyu Y, Zhang Y, Liu Y, Chen W, Zhang X, Xu W, et al. Analysis of potential disruptive technologies in the electronics and information field towards the intelligent society. Engineering 2021;7(8):1051–6.